Analysis of Standby Power in an Enclosed High-Speed Flywheel Energy Storage System Using the CFD-ANOVA Approach

Mahmoud Eltaweel and Mohammad Reza Herfatmanesh

School of Physics, Engineering and Computer Science, University of Hertfordshire

ABSTRACT

During urban driving, a significant amount of energy is lost due to continuous braking, which can be recovered and stored. The flywheel energy storage system (FESS) can efficiently recover and store the vehicle's kinetic energy during deceleration. However, standby losses in FESS, primarily due to aerodynamic drag, can affect its overall efficiency. To address this issue, the flywheel rotor is typically housed in a dedicated housing maintained at a low pressure using a vacuum pump. Standby power is known as the total power used by the auxiliary systems and the power needed to overcome drag and keep the flywheel rotor at a specific state of charge. The Analysis of Variance (ANOVA) technique was combined with the computational fluid dynamics (CFD) technique in this study to determine the optimal flywheel design parameters and investigate their impact on standby power. The study's results demonstrated the optimal combination of the airgap size and the rotor's pressure cavity to achieve the lowest standby power.

INTRODUCTION

Urban driving contributes significantly to energy consumption and greenhouse gas emissions. Braking during urban driving results in significant energy loss, which can be recovered and stored for future use. The flywheel energy storage system (FESS) is a novel technology that efficiently recovers and stores kinetic energy generated during vehicle deceleration [1]. The stored energy can then accelerate the vehicle, reducing reliance on fossil fuels and lowering carbon dioxide emissions [2]. However, FESS systems also have a drawback in the form of aerodynamic drag, also known as windage. Windage occurs when air friction and turbulence affect the spinning flywheel rotor, leading to losses in stored energy. Windage loss contributes significantly to total losses in high-speed rotating machines, increasing self-discharge and reducing FESS' overall efficiency and effectiveness. As a result of windage loss, FESS may be unsuitable for long-term energy storage applications [2]. To minimise windage, the flywheel rotor is housed in a dedicated housing maintained at a low pressure using a vacuum pump [3]. The power the vacuum pump uses to maintain the low-pressure environment and the power needed to overcome drag is known as standby power. Standby power, along with the power needed to keep the flywheel rotor at a specific state of charge, is a crucial factor in determining the overall efficiency of the FESS [3], [4].

Several studies have investigated approaches to reducing windage loss in FESS [1]. The use of various materials to improve FESS performance and various design approaches for minimising windage loss has been the focus of research [5]. Furthermore, computational fluid dynamics (CFD) has been studied as a tool for modelling and analysing flow in the annulus of a solid FESS to identify strategies for improving the system's overall efficiency and effectiveness [6], [7]. Additionally, Taylor-Couette flow has been explored to examine flow stability in the annular gap and the heat transfer properties to reduce losses. The heat produced by aerodynamic losses can influence the performance and lifespan of high-speed FESS. To reduce windage loss and improve the thermal performance of rotating machinery, examining the flow stability in an annular gap and the heat transfer properties is an efficient way, as stated in [8].

Anderson [9] presented the results of windage loss in a high-speed motor using a commercial CFD software package. Their research provided a method for designers to quickly assess the impact of windage loss on the thermal performance of rotating machinery. Windage loss in high-speed motors can be reduced using a new structure that combines an aerodynamic step thrust bearing with a spiral-grooved viscous vacuum pump, as stated by Asami et al. [3]. According to Nachouane et al. [7], calculating windage loss heavily relies on the skin friction coefficient, a non-dimensional parameter affected by the radius ratio and the Reynolds number. The windage losses produced are very different in large and small gaps. To qualify as having a small gap, a ratio must have a gap/diameter of less than 0.005 to 0.02 [10]. Investigations into windage losses for large gaps and atmospheric air have been the subject of numerous studies [11]. Numerous researchers have started using CFD numerical simulations in conjunction with experiments in recent years [12]–[16]. In a vacuum chamber, Walton et al. [10] investigated the windage losses of a rotor supported by gas foil bearings, but they did not consider the fluid field's impact near the journal.

A vacuum-tight seal is a crucial component of a FESS to maintain a low-pressure environment [17]. Mechanical, magnetic, and labyrinth seals are commonly used for this purpose. Mechanical seals comprise two metal surfaces held together by spring pressure to form a vacuum-tight seal. Magnetic seals are more expensive than mechanical seals but can handle high-speed rotation or vibration using magnetic

force [18]. Labyrinth seals use grooves and ridges to form a barrier and are less expensive but may be less reliable than other seals [19]. The vacuum pump used in a FESS is another critical component for maintaining the low-pressure environment [20]. Different types of pumps are available, and the selection depends on the system's specific requirements and desired vacuum level [21]. Mechanical pumps, such as rotary vane and piston pumps, are most widely used due to their affordability, compactness, ultimate high vacuum, and dust and particulate matter resistance. Cryogenic pumps can achieve higher vacuums but are more expensive and require specialised equipment, while molecular turbo pumps are highly efficient and expensive. Rotary vane and piston pumps are most suitable for low to medium vacuum applications [22].

FESS supports the rotor with air or magnetic bearings to achieve low friction. Air bearings, also known as aerostatic bearings, use pressurised air to provide low-friction levitation, allowing for precise control and extending system longevity by eliminating physical contact between moving parts [23]. Magnetic bearings use a magnetic field for levitation, which provides high accuracy and longevity but is more complicated and expensive. To achieve optimal vacuum tightness and longevity, both types of bearings can be combined with various seals, such as mechanical or magnetic seals [24].

This study aims to determine the optimal flywheel design parameters that minimise the standby power in FESS. The Analysis of Variance (ANOVA) technique was used to investigate the effect of two parameters on standby power: airgap size and operating pressure. These parameters were modelled using computational fluid dynamics (CFD), allowing for a thorough examination of the relationships between the parameters and standby power. The findings of this study can be used to develop FESSs with lower standby power and higher energy efficiency. To the authors' knowledge, this is the first attempt to investigate the effect of airgap size and operating pressure while considering the FESS's standby power. This study is significant because it applies to the automotive industry and other fields in which FESSs are used, such as renewable energy storage, aerospace, and military applications.

NUMERICAL MODELLING

NUMERICAL MODEL SETUP

This study proposes a numerical model of a solid flywheel with a uniform, concave, and closed airgap to investigate the effect of airgap size and operating pressure on standby power in FESSs. To predict the skin friction coefficient and describe the airgap flow structure, CFD methods are used. The governing equations that a CFD code uses are based on equations for the conservation of fluid motion that adhere to the fundamental principles of fluid mechanics, including energy, momentum, and mass conservation laws [25] [26]. The FESS CFD domain is created and divided into computational cells and nodes. After the mesh is established, the governing equations are numerically discretised to a system of linear algebraic equations [27]. The following are governing equations for a turbulent flow in the steady state which is outlined as follows [28]:

Continuity equation:

$$\frac{\partial \rho}{\partial t} + \nabla . \rho V = 0 \quad (1)$$

Momentum equation:

$$\frac{D(\rho V)}{Dt} = -\nabla p + \nabla \cdot \tau_{ij} + \rho g \quad (2)$$

Energy equation:

$$\frac{D(\rho C_p T)}{Dt} = \nabla \cdot (\lambda \nabla T) + \Phi \quad (3)$$

Where V is the velocity vector, ρ is the density, ∇p is the pressure force, $\nabla \cdot \tau_{ij}$ is the viscous force, ρg is the gravitational force, $\nabla \cdot (\lambda \nabla T)$ is the heat conduction through the fluid element boundaries, λ is the thermal conductivity, *T* is the temperature, and Φ is the heat from the conversion of mechanical energy. The CFD simulation of a fluid depends on the Knudsen number, which determines whether the flow of a fluid can be modelled using continuum mechanics or requires statistical mechanics [3]. This study used a Knudsen number less than 0.01 to keep the flow continuous and allow the use of Navier-Stokes equations.

BOUNDARY CONDITIONS

For this study, ANSYS Fluent was utilised as the CFD program to model the FESS, which consists of a cylindrical rotor, a housing, and an air gap between them (see Figure 1(a)). The rotor's radius and length were fixed at 0.08 m, and periodic boundary conditions were applied to all periodic surfaces as the FESS flow pattern allows for periodic regions [29]. To reduce computational resources and costs, an 8°-slice from the FESS with a symmetry plane in the centre was simulated. Figure 1(b) shows the simplified geometry with the periodic region and symmetry plane.

To ensure the accuracy and reliability of numerical simulations, performing a mesh independence analysis is crucial. A structured quadrilateral mesh was utilized to simulate a system consisting of a rotor and housing, both varying in size from 1 to 2mm, along with an airgap ranging from 0.1 to 0.2mm. A mesh independence test was conducted to identify the optimal mesh for the simulations, using the highest studied rotational speed of 4000 rad/s to analyse the average air temperature, rotor, and housing temperature. Additionally, a 3D steady-state turbulent flow model utilising a moving reference frame (MRF) was used to examine the system's steady-state performance. This approach resolves most flow characteristics, including mass flow rates and pressure changes across the rotating components [30]. Because the Reynolds number in the air gap was in the turbulent region for the rotational speeds studied, a turbulence model was required. The SST K- ω turbulence model was used to solve the Reynolds-averaged Navier-Stokes (RANS) equations. This model is suitable for estimating fluid flow and heat transfer in concentric cylinder systems, as demonstrated in the existing literature on turbulence modelling of Taylor-Couette flow in high-swirl narrow annulus gaps [9], [32], [33].

Sutherland's three equations were employed to calculate air viscosity, assuming ideal gas properties.

The system had no inlet or outlet, and the overall thermal boundary condition of the housing was set to 24°C. A high-resolution boundary layer mesh with $y_+ \leq 1$ was created to resolve the viscous sublayer.

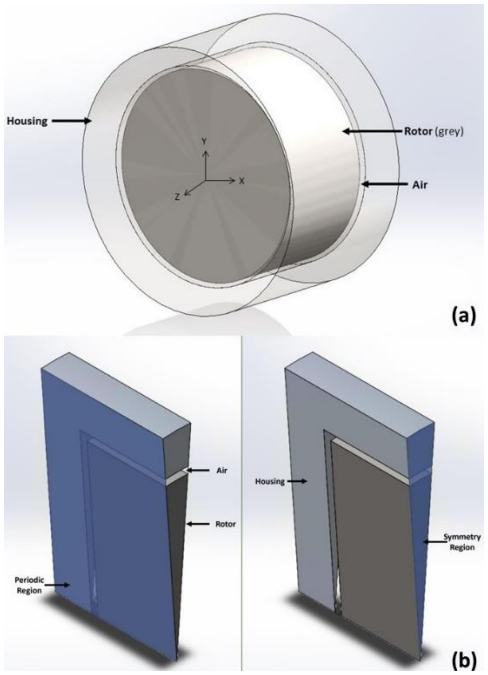

Figure 1 Numerical domain, (a) FESS geometry in 3D, (b) the simplified geometry with periodic and symmetry region

NUMERICAL MODEL VALIDATION

The comparison of skin friction coefficient variation to experimental data is a crucial step in verifying the accuracy and validity of the numerical simulation. This study compared the skin friction coefficient and Taylor number distributions obtained from the CFD model to the experimental data presented by Castle and Mobbs [33] and SIONG [34]. The results, shown in Figure 3, demonstrate that the critical Taylor numbers determined numerically are in excellent agreement with the previously published data in the literature. Moreover, the CFD model accurately represents the distribution of skin friction coefficients in the first zone, and the estimated skin friction coefficients closely follow the data presented by Castle and Mobbs [33] and SIONG [34] when Taylor vortices form in the airgap. These results suggest that the CFD model's predictions closely match the experimental data and provide confidence in the accuracy of the simulation. On the other hand, the CFD model was validated by the authors' experimental work [35]. The experimental and numerical results agree well, with both methods exhibiting similar trends. The differences between experimental and numerical results are within a 15% margin of error.

PARAMETRIC STUDY

Analysis of variance (ANOVA) is a statistical tool that can be used to learn about the relationships between variables and the effects of each variable on the experiment and their interactions [36]. ANOVA would aid in determining the significance of the studied FESS parameters and their effects on achieving optimal standby power.

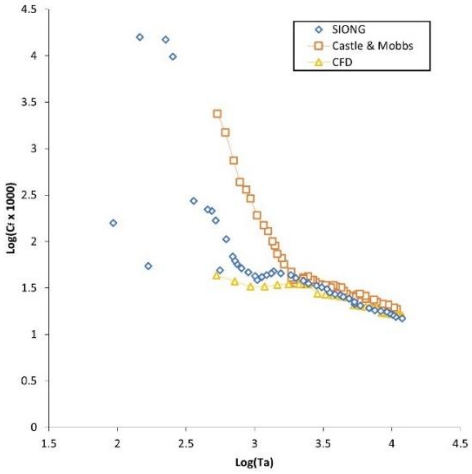

Figure 2 Rotor skin friction coefficient (Cf) vs Taylor number (Ta) validation

RESPONSES SELECTION

The selection of system responses serves the purpose of exemplifying the local shape of the response surface through the simulation of the interaction and effects of the system parameters. Additionally, these responses are utilised to evaluate the system's capabilities and limitations and identify the optimal system settings [37]. In this study, the focus is on analysing the standby power of the FESS. Standby power is the sum of windage losses and the power required to maintain a low-pressure environment by the vacuum pump. Reduced standby power reduces the system's self-discharging rate, making it an ideal solution for extended storage periods, which can be useful for various applications.

FACTORS SELECTION

To reduce the windage losses, the flywheel rotor is typically housed in a dedicated housing maintained at a low pressure using a vacuum pump. The outer rotor and inner housing surface temperatures of a high-speed rotating machine can be significantly influenced by windage losses caused by non-ventilated airflows within the annulus of a FESS. Increased airgap size is commonly used to reduce temperature; however, this leads to higher power required by the vacuum pump to create a low-pressure environment. Hence, the airgap size and the rotor cavity pressure are two key factors that require consideration when designing a FESS. In order to meet the requirement of a compact system suitable for a range of applications, the study selected five different airgap sizes to achieve a narrow gap between the rotor and housing. The parameter used in this study to define the airgap is a dimensionless parameter called the radius ratio, which is $\eta = r_o/r_h$ where r_o is the rotor radius and r_h is the internal housing radius. The rotational velocity of the rotor was limited to 4000 rad/s to ensure safety, which is the maximum allowable velocity for a solid cylinder rotor with a factor of safety of two when the rotor's material is steel 4340 [38]. To minimise windage losses, it is essential to maintain a low-pressure environment around the rotor cavity. However, a hard vacuum is not ideal as it would require considerable power from the vacuum pump and make maintenance more challenging. A partial vacuum can reduce the FESS's

windage losses while also being achieved using cheap and less complex vacuum pumps such as rotary vane pumps. Five different rotor cavity pressures were used in this study, ranging from atmospheric pressure to 200 mbar. A DC rotary vane pump with 24 V was used in the study to achieve the required partial vacuum [39]. The different values of each studied level are shown in Table 1.

Table 1 The factors studied with different levels

Levels	Factors	
	A	B
	Airgap [mm] (η)	Rotor cavity pressure [mbar]
1	1 (0.99)	1000
2	2 (0.975)	800
3	3 (0.96)	600
4	4 (0.95)	400
5	5 (0.94)	200

ANALYSIS SETUP

In this study, the ANOVA used factorial analysis to determine the effects of the two factors on responses at different levels [36]. This method allows researchers to rank variables according to their influence on objective function values [40] [41]. This analysis can be used for FESS optimisation to determine which parameters affect performance and optimise those parameters to achieve the desired standby power value. The main processes in optimisation are estimating the coefficients in a mathematical model, forecasting the response, and determining the model's suitability. Regression analysis of the data was performed using the statistical software Design-Expert, to fit the proposed equations and plot response surfaces.

RESULTS AND DISCUSSION

INFLUENCE OF THE AIRGAP SIZE

This study investigates the flow characteristics of cylindrical annulus airgap and the effect of airgap size on windage losses in the studied system. The Taylor number is calculated based on geometrical factors, operational conditions, and fluid characteristics to characterise the airgap flow regimes. The primary factors affecting the flow characteristics are the rotor's rotational speed and the airgap size. When the Taylor number exceeds a critical value, laminar flow collapses, and Taylor instabilities arise, forming counterrotating vortices along the axial direction known as Taylor vortices.

The effect of airgap size on the windage losses of the system is investigated at a rotational velocity of 4000 rad/s. The results show that the current Taylor number consistently exceeds the critical Taylor number, indicating the existence of Taylor vortices in the studied case. The air velocity distribution within the studied airgap size under atmospheric pressure exhibits a spike-shaped flow caused by creating a Taylor-Couette flow in the airgap. The air velocity closest to the housing is near zero, while the velocity closest to the rotor is the greatest.

Furthermore, the airgap size determines the number of Taylor vortices, with larger airgap sizes resulting in fewer Taylor vortices. The Taylor vortices cells take a cubic shape, and their number decreases from 64 to 12 as the airgap size increases from 1 to 5 mm, respectively. The number of Taylor cells decreases dramatically as the airgap size increases, resulting in better heat transfer between the rotor, housing, and air, which leads to lower temperatures for each component and lower windage losses. Figure 3 shows that the number of Taylor cells decreases as the airgap size increases, confirming the above observation. The flow characteristics inside the system are altered upon reducing the cavity pressure. In particular, the presence of Taylor vortices remains unaffected as the air particles remain within the system. However, the reduced pressure results in a lower number of air particles, leading to a decrease in fluid density. This reduction in fluid density reduces the occurrence of viscous friction between the rotor and the air.

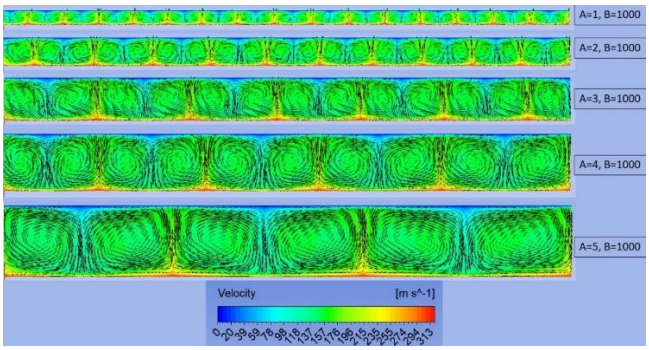

Figure 3 Air velocity distribution inside the studied airgap sizes at atmospheric pressure where (A) is the airgap size in mm and (B) is the rotor cavity pressure in mbar

RESPONSE

An analysis of variance was performed on the chosen response, and the results of the significant factors and their interactions are shown in Table 2. With an F-value of 1483.29, the ANOVA for the response surface quadratic model for standby power revealed that the model was significant. P-values less than 0.05 are considered significant for model terms. Model terms with values greater than 0.10 are deemed unimportant. Therefore, the table responses are significant, and the insignificant factors were removed to improve the model. The F-values for each factor and their interactions are calculated to determine the significance of their mean variation. The tables calculate the relevant P-values with a 95% confidence interval. Statistical results show that these models accurately predicted standby power across the studied variables. Table 2 shows that each factor has a p-value less than 0.05 and is, therefore, significant.

MODEL ADEQUACY

A mathematical model in a regression model describes the relationship between the input variables and the dependent response. The fit statistics for the initial response calculated using Design-Expert

software are shown in Table 3. With only a few data points separating the regression line and the response points, the coefficient of determination (R^2) for regression analysis for the response is 0.9949. The adjusted R^2, which considers unnecessary and valuable parameters, was used to represent the model's variability. The adjusted R^2 value is 0.9968, indicating that only a small percentage of variance was introduced. The predicted R^2 can be used to assess the model's ability to forecast new observations. The results show a 0.2 difference between the adjusted and predicted R^2 values, implying a reasonable correlation. While acceptable precision evaluates the data's signal-to-noise ratio, insufficient precision only evaluates noise. This means a sufficient signal was obtained with a satisfactory precision ratio of 116.718.

Table 2 ANOVA for response surface quadratic model for standby power

Source	Sum of Squares	df	Mean Square	F-value	p-value	
Model	7.589E+05	5	1.518E+05	1483.29	< 0.0001	significant
A-Airgap	16094.69	1	16094.69	157.29	< 0.0001	
B-Pressure Level	7.295E+05	1	7.295E+05	7129.50	< 0.0001	
AB	7093.68	1	7093.68	69.33	< 0.0001	
A²	2882.71	1	2882.71	28.17	< 0.0001	
B²	3290.06	1	3290.06	32.15	< 0.0001	
Residual	1944.14	19	102.32			
Cor Total	7.608E+05	24				

Table 3 The fit statistics for the obtained response

Std. Dev.	10.12	**R²**	0.9974
Mean	734.51	**Adjusted R²**	0.9968
C.V. %	1.38	**Predicted R²**	0.9949
		Adequate Precision	116.7178

STANDBY POWER RESPONSE

This study evaluates the FESS's standby power, which is the sum of windage losses, and the power required for maintaining a low-pressure environment. Decreasing standby power reduces the self-discharging rate of the system, making it well-suited for extended storage periods in various applications. The viscous friction between the rotor and the air in the gap during rotation generates windage losses. The size of the airgap and the thermophysical properties of the fluids involved influences the losses. In this system, the stationary outer cylinder acts as the housing, while the inner cylinder is the rotating rotor. As the rotational speed increases, the air velocity distribution changes due to the Taylor number exceeding the critical value of 41.3, creating the Taylor vortex.

The windage loss of an enclosed flywheel can be expressed as the sum of two components: aerodynamic loss due to skin friction, which arises from the viscous forces acting on the flywheel's outer surface, and aerodynamic loss due to flywheel torque, which arises from the flow interaction between the flywheel sides and the housing. The total windage loss can be calculated using equation (4) [35]:

$$P = (\pi \times L \times C_f \times \rho \times {r_i}^4 \times \Omega^3) + (C_m \times \rho \times {r_i}^5 \times \Omega^3) \quad (4)$$

Where P is the total windage loss in watts, L is the flywheel width in metres, ρ is the gas density in kilogrammes per cubic metre, r_i is the flywheel radius in metres, Ω is the flywheel's rotational velocity in rad per second, C_f is the skin friction coefficient on the top flywheel surface, and C_m is the flywheel disk torque coefficient on the sides of the flywheel. C_f and C_m can be determined using numerical simulations based on the average gas temperature within the flywheel airgap. The windage losses with respect to the rotational velocity from 40,000 rpm to 0 rpm with 1000 intervals for all studied simulations are shown in Figure 4.

The research findings show that larger air gaps lead to lower air friction and hence, reduced windage losses. This is due to the increased rotor shear stress in smaller air gaps, further amplified by the formation of Taylor vortices. Taylor vortices appear more frequently as the airgap widens, while Taylor cells are less rapidly affected by azimuth waves as the airgap narrows [42]. The highest windage losses are observed at atmospheric pressure and can be significantly reduced by reducing the pressure within the cavity. while the lowest windage losses were achieved with the largest studied airgap size and the lowest cavity pressure.

Several factors must be considered when calculating the power required to run a vacuum pump to reduce the pressure inside a FESS. First, the desired vacuum level must be determined. The second step is to choose a vacuum pump, a Dual-stage, high-performance rotary vane pump with a pumping speed of 2.5 m^3/h (Duo 3 DC, 24 V DC, DN 16 ISO-KF) that can be used in vehicles [39]. The third factor is the type of seal and bearing used to maintain the vacuum. Finally, there is the volume of gas contained within the rotor cavity. The calculation of time the pump would run to achieve the required pressure level can be calculated using the following formula [43]:

$$t = \frac{V}{S} \times \ln \frac{P_1}{P_2} \quad (5)$$

Where V is the volume of the rotor's cavity, S is the pumping rate of the selected vacuum pump, P_1 is the initial pressure in the FESS, and P_2 is the required pressure. The power required to run the pump is 240 W [39], but because the system's seal and bearing would affect the pressure level, the vacuum pump must regulate the pressure inside the cavity to ensure a constant pressure level.

It was found that reducing cavity pressure and

increasing airgap size effectively reduced windage losses. However, it was observed that increasing airgap size resulted in increased power consumption by the vacuum pump to achieve the desired pressure level. Moreover, increasing airgap size was observed to be beneficial for reducing standby power consumption when the pressure inside the FESS was atmospheric or more than 600 mbar, as shown in Figure 5. Conversely, when the pressure was below 400 mbar, the minimum standby power was achieved at around 2 mm airgap size due to the increased power required to achieve the desired pressure level for a larger cavity.

The regression model for predicting the standby power is presented using the ANOVA as equation (6). Note that the R^2 value for this regression model is 99.7%. To obtain accurate predictions, the original units of each factor must be specified. The response prediction equation represents a valuable tool for predicting the response variable, and it can be used to predict the standby power for pressure levels between atmospheric pressure to 200 mbar and airgap size between 1 to 5mm.

$$P_t = 347.09 - 31.17791A + 0.935957B - 0.042112AB + 6.41729A^2 - 0.000171B^2 \quad (6)$$

Where P_t is the standby power in watts, A is the airgap size in mm, and B is the cavity pressure in mbar.

OPTIMISATION

Myers and Montgomery [44] introduce the term "desirability" to refer to the multiple-response method. The desirability function, denoted as *D(X)*, is the objective function employed in this method. For each response, an ideal range, d_i, is specified, with the most desirable range between zero and one (representing the least to the most desirable values, respectively). The simultaneous objective function in this method is determined as the geometric mean of all the transformed responses, as shown in equation (7):

$$D = (d_1 \cdot d_2 \cdot \dots d_n)^{\frac{1}{n}} = (\prod_{i=1}^{n} d_i)^{\frac{1}{n}} \quad (7)$$

Where the number of measured responses is *n, f*rom zero outside the limits to one at the goal, desirability is an objective function. A point is found that maximises the desirability function by using numerical optimisation. Adjusting the weight or importance of a goal can change the goal's characteristics. A single desirability function is applied to various responses and factors, and numerical optimisation is used to find the maximum value of the desirability function. The Design-Expert software is used for numerical optimisation for the system response. The software provides a solution that can achieve the highest desirability by minimising standby power, considering the importance of each factor.

Based on the optimisation, the proposed solution achieves the lowest standby power at a pressure level of 200 mbar and an airgap size of 2.37 mm, with a desirability of 1. The results are presented in Figure 6. To ensure that the predicted values can be used and are compatible with the results obtained from CFD simulations, the predicted standby power for the proposed solution is validated by running a CFD simulation. As a result, the numerical and predicted values are in good agreement, with a difference of 3%.

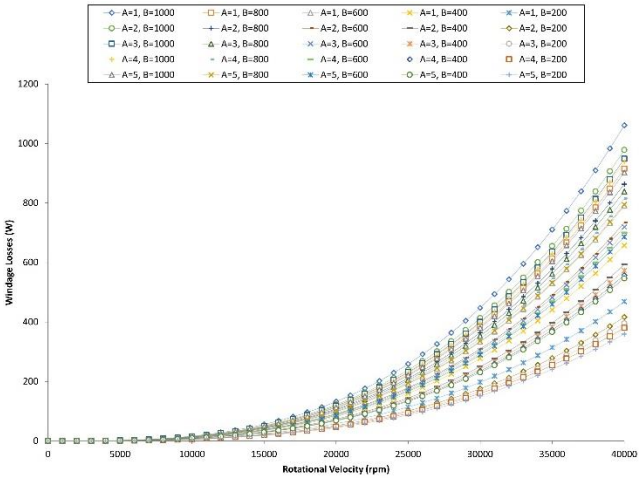

Figure 4 The windage losses with respect to rotational velocity for the 25 runs, where (A) is Airgap size in mm and (B) is the rotor cavity pressure in mbar.

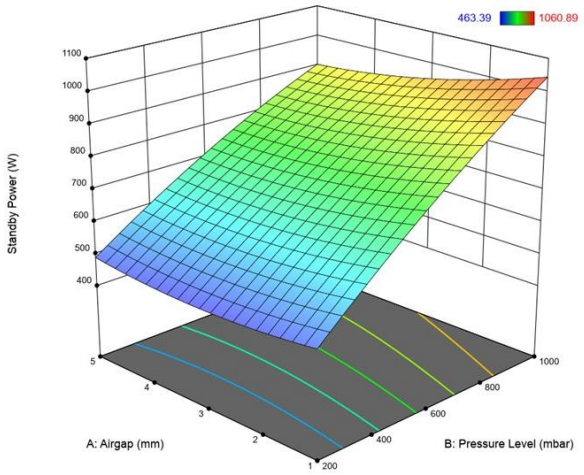

Figure 5 3D plot for standby power between airgap size and pressure level

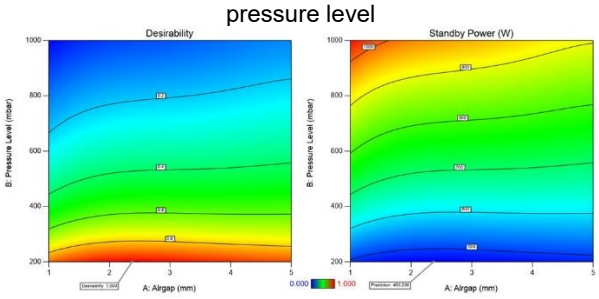

Figure 6 The desirability of the optimisation of the FESS and the corresponding standby power

CONCLUSION

The flywheel energy storage system (FESS) presents an efficient solution for recovering and storing kinetic energy lost during deceleration in urban driving scenarios. However, standby losses in FESS, predominantly due to aerodynamic drag, can harm its overall efficiency. The FESS is typically enclosed in a dedicated housing maintained at low pressure using a vacuum pump to address this issue. The current study utilised the Analysis of Variance (ANOVA) method and extensive CFD simulations to investigate the optimal design parameters that minimise standby power. The results showed that the airgap size and the rotor's

cavity pressure significantly affect standby power, and an optimal combination of these parameters can achieve the lowest standby power for the FESS. The lowest standby power was attained when the system operated at a pressure level of 200mbar, accompanied by an airgap size of 2.37 mm. These findings can be utilised to improve the efficiency and performance of FESS in urban driving scenarios, paving the way for future research and advancements in the automotive industry towards more energy-efficient flywheel designs. This will lead to reduced emissions and more environmentally friendly driving experiences.

ACKNOWLEDGMENTS

This work is supported by the European Union's Horizon 2020 research and innovation programme under the Marie Skłodowska-Curie grant agreement No 801604.

REFERENCES

[1] A. K. Arani, H. Karami, G. Gharehpetian, and M. Hejazi, ‘Review of Flywheel Energy Storage Systems structures and applications in power systems and microgrids’, *Renew. Sustain. Energy Rev.*, vol. 69, pp. 9–18, 2017.

[2] M. E. Amiryar and K. R. Pullen, ‘A review of flywheel energy storage system technologies and their applications’, *Appl. Sci.*, vol. 7, no. 3, p. 286, 2017.

[3] F. Asami, M. Miyatake, S. Yoshimoto, E. Tanaka, and T. Yamauchi, ‘A method of reducing windage power loss of a high-Speed motor using a viscous vacuum pump’, *Precis. Eng.*, vol. 48, pp. 60–66, 2017.

[4] T. Engel and D. Braid, ‘High-speed motor for use in an ultrahigh-vacuum environment’, *Rev. Sci. Instrum.*, vol. 56, no. 8, pp. 1668–1669, 1985.

[5] M. E. Amiryar and K. R. Pullen, ‘Analysis of standby losses and charging cycles in flywheel energy storage systems’, *Energies*, vol. 13, no. 17, p. 4441, 2020.

[6] M. L. Hosain, R. B. Fdhila, and K. Rönnberg, ‘Air-gap flow and thermal analysis of rotating machines using CFD’, *Energy Procedia*, vol. 105, pp. 5153–5159, 2017.

[7] A. Nachouane, A. Abdelli, G. Friedrich, and S. Vivier, ‘Estimation of windage losses inside very narrow air gaps of high speed electrical machines without an internal ventilation using CFD methods’, presented at the 2016 XXII International Conference on Electrical Machines (ICEM), 2016, pp. 2704–2710.

[8] D.-D. Dang, X.-T. Pham, P. Labbe, F. Torriano, J.-F. Morissette, and C. Hudon, ‘CFD analysis of turbulent convective heat transfer in a hydro-generator rotor-stator system’, *Appl. Therm. Eng.*, vol. 130, pp. 17–28, 2018.

[9] K. R. Anderson, J. Lin, C. McNamara, and V. Magri, ‘CFD study of forced air cooling and windage losses in a high speed electric motor’, *J. Electron. Cool. Therm. Control*, vol. 5, no. 02, p. 27, 2015.

[10] J. F. Walton, H. Heshmat, and M. Tomaszewski, ‘Power Loss in High-Speed Micro Turbomachinery: An Experimental Study’, presented at the Turbo Expo: Power for Land, Sea, and Air, 2012, vol. 44717, pp. 871–880.

[11] C. Wei *et al.*, ‘Research on windage losses of smooth rotor supported by active magnetic bearings in a vacuum chamber’, *Vacuum*, vol. 159, pp. 76–81, 2019.

[12] A. Rasekh, P. Sergeant, and J. Vierendeels, ‘Development of correlations for windage power losses modeling in an axial flux permanent magnet synchronous machine with geometrical features of the magnets’, *Energies*, vol. 9, no. 12, p. 1009, 2016.

[13] M. L. Hosain and R. B. Fdhila, ‘Air-gap heat transfer in rotating electrical machines: a parametric study’, *Energy Procedia*, vol. 142, pp. 4176–4181, 2017.

[14] M. L. Hosain, R. B. Fdhila, and K. Rönnberg, ‘Taylor-Couette flow and transient heat transfer inside the annulus air-gap of rotating electrical machines’, *Appl. Energy*, vol. 207, pp. 624–633, 2017.

[15] E. E. Swanson, P. S. O’Meara, and H.-H. Tsuei, ‘Annular Gap Windage Loss Measurements for High Speed Electrical Machinery’, presented at the Turbo Expo: Power for Land, Sea, and Air, 2017, vol. 50886, p. V05BT15A005.

[16] E. E. Swanson, H.-H. Tsuei, and P. S. O’Meara, ‘The Effect of Axial Flow Velocity on Annular Gap Windage Power Loss’, presented at the Turbo Expo: Power for Land, Sea, and Air, 2017, vol. 50794, p. V02BT42A002.

[17] L. Matuszewski, ‘New designs of centrifugal magnetic fluid seals for rotating shafts in marine technology’, *Pol. Marit. Res.*, vol. 26, no. 2, pp. 33–46, 2019.

[18] K. Kalista, J. Liska, and J. Jakl, ‘A vibration sensor-based method for generating the precise rotor orbit shape with general notch filter method for new rotor seal design testing and diagnostics’, *Sensors*, vol. 21, no. 15, p. 5249, 2021.

[19] K. M. Katcher, T. Revak, A. Rimpel, J. Ratay, and K. Brun, ‘Abradable Seal Test Rig for Quantifying Abradable Material Performance During Labyrinth Seal Rubs in Centrifugal Compressors: Design and Test Results’, presented at the Turbo Expo: Power for Land, Sea, and Air, 2022, vol. 86052, p. V007T19A005.

[20] M. Strasik *et al.*, ‘An overview of Boeing flywheel energy storage systems with high-temperature superconducting bearings’, *Supercond. Sci. Technol.*, vol. 23, no. 3, p. 034021, 2010.

[21] T. M. Adams and R. A. Layton, ‘Introductory Mems’, *Fabrication and*, 2010.

[22] X. Li, N. Erd, and A. Binder, ‘Evaluation of flywheel energy storage systems for residential photovoltaic installations’, presented at the 2016 International symposium on power electronics, electrical drives, automation and motion (SPEEDAM), 2016, pp. 255–260.

[23] H. Wang, Z. Wu, K. Liu, J. Wei, and H. Hu, ‘Modeling and control strategies of a novel axial

hybrid magnetic bearing for flywheel energy storage system', *IEEEASME Trans. Mechatron.*, vol. 27, no. 5, pp. 3819–3829, 2022.
[24] T. S. Slininger, W. Chan, E. L. Severson, and B. Jawdat, 'An overview on passive magnetic bearings', presented at the 2021 IEEE International Electric Machines & Drives Conference (IEMDC), 2021, pp. 1–8.
[25] N. Regalado-Rodríguez and C. Militello, 'Comparative study of the effects of increasing heat transfer area within compression and expansion chambers in combination with modified pistons in Stirling engines. A simulation approach based on CFD and a numerical thermodynamic model', *Energy Convers. Manag.*, vol. 268, p. 115930, 2022.
[26] B. Andersson, R. Andersson, L. Håkansson, M. Mortensen, R. Sudiyo, and B. Van Wachem, *Computational fluid dynamics for engineers*. Cambridge university press, 2011.
[27] J. Tu, G. H. Yeoh, and C. Liu, 'Chapter 3 - Governing Equations for CFD—Fundamentals', in *Computational Fluid Dynamics*, J. Tu, G. H. Yeoh, and C. Liu, Eds. Burlington: Butterworth-Heinemann, 2008, pp. 65–125. doi: 10.1016/B978-075068563-4.50005-7.
[28] T. L. Bergman, T. L. Bergman, F. P. Incropera, D. P. Dewitt, and A. S. Lavine, *Fundamentals of heat and mass transfer*. John Wiley & Sons, 2011.
[29] K. Ryu and K.-S. Lee, 'Generalized heat-transfer and fluid-flow correlations for corrugated louvered fins', *Int. J. Heat Mass Transf.*, vol. 83, pp. 604–612, 2015.
[30] J. D. Anderson and J. Wendt, *Computational fluid dynamics*, vol. 206. Springer, 1995.
[31] C. Jungreuthmayer *et al.*, 'A detailed heat and fluid flow analysis of an internal permanent magnet synchronous machine by means of computational fluid dynamics', *IEEE Trans. Ind. Electron.*, vol. 59, no. 12, pp. 4568–4578, 2011.
[32] D. A. Howey, A. S. Holmes, and K. R. Pullen, 'Measurement and CFD prediction of heat transfer in air-cooled disc-type electrical machines', *IEEE Trans. Ind. Appl.*, vol. 47, no. 4, pp. 1716–1723, 2011.
[33] P. Castle and F. Mobbs, 'Paper 6: Hydrodynamic Stability of the Flow between Eccentric Rotating Cylinders: Visual Observations and Torque Measurements', presented at the Proceedings of the Institution of Mechanical Engineers, Conference Proceedings, 1967, vol. 182, no. 14, pp. 41–52.
[34] L. S. SIONG, 'An experimental investigation of taylor couette flow between eccentric cylinders', 2007.
[35] S. Motaman, M. Eltaweel, M. R. Herfatmanesh, T. Knichel, and A. Deakin, 'Numerical analysis of a flywheel energy storage system for low carbon powertrain applications', *J. Energy Storage*, vol. 61, p. 106808, May 2023, doi: 10.1016/j.est.2023.106808.
[36] H. Scheffe, *The analysis of variance*, vol. 72. John Wiley & Sons, 1999.
[37] M. Eltaweel *et al.*, 'Application of the ANOVA method in the optimization of a thermoelectric cooler-based dehumidification system', *Energy Rep.*, vol. 8, pp. 10533–10545, Nov. 2022, doi: 10.1016/j.egyr.2022.08.193.
[38] Y. Han, Z. Ren, and Y. Tong, 'General Design Method of Flywheel Rotor for Energy Storage System', *2012 Int. Conf. Future Energy Environ. Mater.*, vol. 16, pp. 359–364, Jan. 2012, doi: 10.1016/j.egypro.2012.01.059.
[39] 'Standard | Pfeiffer Vacuum'. https://www.pfeiffer-vacuum.com/en/products/vacuum-generation/rotary-vane-pumps/two-stage/standard/16158/duo-3-dc-24-v-dc-dn-16-iso-kf (accessed Feb. 27, 2023).
[40] M. Tabatabaei, A. Lovison, M. Tan, M. Hartikainen, and K. Miettinen, 'ANOVA-MOP: ANOVA decomposition for multiobjective optimization', *SIAM J. Optim.*, vol. 28, no. 4, pp. 3260–3289, 2018.
[41] M. G. Larson, 'Analysis of variance', *Circulation*, vol. 117, no. 1, pp. 115–121, 2008.
[42] M. Fénot, Y. Bertin, E. Dorignac, and G. Lalizel, 'A review of heat transfer between concentric rotating cylinders with or without axial flow', *Int. J. Therm. Sci.*, vol. 50, no. 7, pp. 1138–1155, 2011.
[43] 'vacuum pump selection and calculation-Vacuum Pump - EVP Vacuum Solution!' https://www.evpvacuum.com/vacuum-pump-selection-and-calculation.html (accessed Feb. 27, 2023).
[44] 'Stat-Ease » v11 » Optimization Overview » Numerical Optimization » Desirability Details'. https://www.statease.com/docs/v11/contents/optimization/desirability-details/ (accessed Mar. 28, 2022).